Charge Transport Characteristics of High Efficiency Dye-Sensitized Solar Cells Based on Electrospun TiO_2 Nanorod Photoelectrodes

Byung Hong Lee,[†,‡] Mi Yeon Song,[†] Sung-Yeon Jang,[†] Seong Mu Jo,[†] Seong-Yeop Kwak,[‡] and Dong Young Kim*[,†]

Center for Energy Materials Research, Korea Institute of Science and Technology, P. O. Box 131 Cheongryang, Seoul 130-650, Korea, and Department of Materials Science and Engineering, Seoul National University, Seoul 151-744, Korea

Received: August 13, 2009; Revised Manuscript Received: November 3, 2009

In this report, dye-sensitized solar cells (DSSCs) with high energy conversion efficiencies were fabricated using TiO_2 nanorods electrospun from a solution mixture of titanium *n*-propoxide and poly(vinyl acetate) in dimethyl formamide. Investigation of the charge transport characteristics of this unique type of DSSC disclosed that the efficiency of the DSSCs was enhanced by optimizing the nanorod morphology to facilitate charge transport. Our TiO_2 nanorods have an intrinsically higher sensitizer loading capability than conventional TiO_2 nanoparticles and have much slower recombination lifetimes compared to conventional nanoparticles. Long electron lifetime in nanorod electrode contributes to the enhanced effective photocarrier collection as well as the conversion efficiency. The electron transport behavior of nanorod photoelectrodes was further improved by $TiCl_4$ post-treatment. The post-treatment reduces the pore volume of nanorod photoelectrodes while improving inter-rod connectivity and enhancing electron diffusion. The electron diffusion coefficient of post-treated nanorod was ~51% higher than that of an untreated one, leading to a charge collection efficiency that was 19% higher at a incident photonflux of 8.1×10^{16} cm^{-2} s^{-1}. Finally, the efficiency of nanorod-based DSSCs was optimized at a photoelectrode thickness of 14 μm to achieve 9.52% under masked illumination of simulated solar light, AM 1.5 Global (V_{oc} = 761 mV, J_{sc} = 17.6 mA cm^{-2}, fill factor = 70.0%).

Introduction

Since the pioneering work of Grätzel and co-workers in 1991, dye-sensitized solar cells (DSSCs) have been considered one of the most promising candidates for renewable energy devices because of their high efficiency and low production cost.[1] In DSSCs, photosensitizers absorb light to generate excited electron−hole pairs that then undergo interfacial charge separation. The separated electrons then propagate through the TiO_2 photoelectrode while the holes diffuse through an electrolyte solution to the counter electrode. The separated electrons and holes must travel a substantial distance, and this charge collection competes with charge recombination that occurs at TiO_2/dye/electrolyte interfaces. To realize optimal device efficiencies, charge diffusion must be enhanced while minimizing charge recombination.[2−4] For TiO_2 photoelectrodes, several parameters such as morphology, pore volume, and the crystallinity of TiO_2 influence the charge transport and recombination processes that control DSSC light-to-electricity conversion efficiencies. For instance, electron transport in widely used mesoporous TiO_2 nanoparticle (NP)-based photoelectrodes is significantly influenced by surface states and particle morphology as well as interparticle connectivity.

One-dimensional (1D) nanostructures (e.g., nanowires, nanorods, nanotubes, nanobelts, cauliflower-shaped structures) have been widely considered to have superior electron transport characteristics compared to conventional NP-based systems.[5−8] Previous studies have demonstrated that electron transport in 1D structures is intrinsically faster than that in NP films; this is because the relatively low junction densities found in 1D nanostructures decrease the ohmic loss within the photoelectrode.[5,6] In the case of pseudosingle-crystalline TiO_2 nanowires, superior sensitizer adsorption has also been reported.[7,8]

Herein, we introduce highly efficient TiO_2 nanorod-based NR-DSSCs and compare charge transport properties to those of typical TiO_2 nanoparticle-based (NP, commercially available P-25) NP-DSSCs. TiO_2 nanorod-based (NR) photoelectrodes were prepared by combining the electrospinning process with sol−gel chemistry, as previously reported by our group.[9] The electron transport time (τ_t), diffusion coefficients (D_n), and recombination lifetime (τ_t) of NR-DSSCs and NP-DSSCs were analyzed using intensity-modulated photocurrent spectroscopy (IMPS) and intensity-modulated photovoltage spectroscopy (IMVS) under the limit of small amplitude light perturbation.[10,11] By optimizing the morphology of TiO_2−NR-based photoelectrodes, both the charge transport characteristics and sensitizer adsorption were optimized and a high efficiency (>11%) was achieved under AM 1.5G light illumination.

Experimental Section

TiO_2 nanorod (NR)-based electrodes were prepared by using the electrospinning technique. In the electrospinning (e-spin) process, the precursor solution was prepared by mixing 8 wt % poly(vinyl acetate) (PVAc, MW of 1.0×10^6 g/mol) in DMF, 0.25 M titanium(IV) *n*-propoxide (TiP, Aldrich), and 0.1 M acetic acid together. After stirring for 2 h, the solution was loaded into a syringe equipped with a 24-gauge stainless steel needle. The spinning rate (30 μL/min) was controlled using a syringe pump (KD Scientific model 220). The electric field (12−15 kV) was applied between a metal orifice and the

* To whom correspondence should be addressed. E-mail: dykim@kist.re.kr.
† Korea Institute of Science and Technology.
‡ Seoul National University.

10.1021/jp907855x
Published on Web 11/25/2009

fluorine-doped tin-oxide (FTO)-coated glass substrate at a distance of 10 cm using a power supply (BERTAN SERIES 205B).

TiO_2 nanoparticle (NP)-based photoelectrodes were prepared using the doctor-blade technique. Specifically, the TiO_2 colloidal solution (P25, Degussa) was spread onto a FTO substrate using a doctor-blade coater. The porosity was controlled by adding the 20 wt % poly(ethylene glycol) (Aldrich, average MW = 10 000 g/mol) and 20 wt % poly(ethylene oxide) (Aldrich, average MW = 100 000 g/mol) to the TiO_2 colloidal solution.

For photosensitization studies, the calcined TiO_2 nanorod electrodes were immersed in an ethanol solution containing purified 3×10^{-4} M *cis*-di(thiocyanato)-*N,N′*-bis(2,2′-bipyridyl-4-carboxylic acid-4′-tetrabutylammonium carboxylate) ruthenium(II) (N719, Solaronix) for 24 h at room temperature. The dye-treated TiO_2 electrodes were rinsed with ethanol and dried under nitrogen flow. The liquid electrolyte was prepared by dissolving 0.6 M of 1-butyl-3-methylimidazolium iodide, 0.03 M of iodine, 0.1 M of guanidinium thiocyanate, and 0.5 M of 4-*tert*-butylpyridine in acetonitrile/valeronitrile (85/15 v/v). The counter electrode was produced by coating FTO glass with a thin layer of a 5 mM solution of H_2PtCl_6 in isopropanol. This coating was heated at 400 °C for 20 min. The two electrodes were sealed together with a hot-melt polymer film (24 μm thick, Surlyn, DuPont). The typical active area of the cell ($\sim$0.26 cm^2) was measured by an image analysis program equipped with a CCD camera. The detailed morphologies of the electrospun TiO_2 nanorods were determined by field emission scanning electron microscopy (FE-SEM, HITACHI S-4100).

Pore volumes were estimated using the Brunauer−Emmett−Teller (BET, Sorptomatic 1990) method, and pore size distributions were determined by the Barrett−Joyner−Halenda (BJH, Sorptomatic 1990) method and the nitrogen desorption branches of the isotherms. Dye desorption experiments were carried out using TiO_2 films coated with the N719 dye prepared from a 0.3 mM ethanolic solution. For each sample, the dye was desorbed from the TiO_2 electrodes by treatment with a certain volume of 0.1 M NaOH (aq); the absorbance of the resulting solution was then quantified with a UV−vis spectrophotometer (Hewlett-Packard 8453). For equal area films with similar thicknesses, the absorbance increases linearly with the concentration of the dye. For all samples the dye has been desorbed into equal volumes of diluted NaOH (aq). The relative difference in absorbance directly translates to the relative difference in dye loading of the TiO_2 surfaces. The thickness of the TiO_2 film was measured using a surface profilometer (TENCOR. P-10).

Photovoltaic characteristics were measured using a Keithley 2400 source meter. A solar simulator (1000 W Xe lamp, Oriel) was employed as the light source, and the light intensity (or radiant power) was adjusted with a Si reference solar cell equipped with a KG-5 filter (Fraunhoffer Institute, Germany) for approximating AM 1.5 global radiation.

IPCEs were measured as a function of wavelength from 350 to 800 nm using a specially designed IPCE system for dye-sensitized solar cells (PV Measurements, Inc.). A 75 W xenon lamp was used as the light source for generating a monochromatic beam. Calibration was performed using a NIST-calibrated silicon photodiode as a standard. IPCE values were collected at a low chopping speed of 5 Hz.

The electron transport time and electron recombination lifetimes were measured by intensity-modulated photocurrent spectroscopy (IMPS) and intensity-modulated photovoltage spectroscopy (IMVS). A diode laser with variable power and modulation control (Coherent Lab-laser, 10 mW, 635 nm) was used as the light source for these studies. Illumination was always incident on the working electrode side of the solar cell. The intensity was measured using a calibrated Si-photodiode. IMVS was performed under open-circuit conditions. The output of the solar cell was connected directly to a lock-in amplifier (Frequency Response Analyzers, Solatron 1260A Impedance/Gain-Phase Analyzer). IMPS was performed under short-circuit conditions by connecting the solar cell via a current amplifier (EG&G PAR 273) to the lock-in amplifier. During the IMVS and IMPS measurements, the cell was illuminated with sinusoidally-modulated light having a small ac component (10% or less of the dc component).

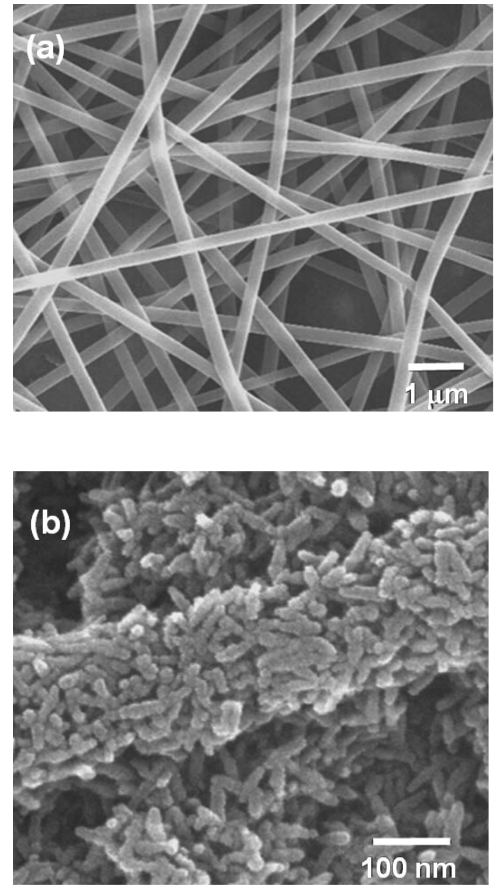

Figure 1. SEM images of electrospun nanofibers: as-spun TiO_2−PVAc nanofibers (a) and TiO_2−NR after calcination at 400 °C (b).

Results and Discussion

TiO_2−NR-based photoelectrodes were prepared by calcining TiO_2 composite fibers that were electrospun from a solution mixture of TiO_2 sol−gel and poly(vinyl acetate) (PVAc) under a high electric field existing between an orifice and a fluorine-doped tin-oxide (FTO)-coated glass plate. The TiO_2−PVAc composite fibers had a diameter of 200−600 nm, as determined from scanning electron microscopy (SEM) images (Figure 1a). In the composite fibers, the TiO_2 phase and PVAc phase were segregated from each other due to their limited miscibility. The as-spun fibers were pretreated under pressure (0.3 MPa) at 120 °C before calcination. Subsequently, calcination at >400 °C in air converted the amorphous TiO_2 to crystalline TiO_2 while the PVAc polymer matrix was removed by thermal decomposition. The resulting nanorods had diameters of $\sim$15 nm and lengths of 60−100 nm. Our previous report showed that TiO_2−NRs are anatase single crystals.[12] SEM images of a TiO_2−NR-based photoelectrode prepared directly on FTO are shown in Figure 1b.

NR-DSSCs were fabricated using a typical procedure with the N719 dye as the sensitizer. To elucidate the unique characteristics of electrospun NR-based photoelectrodes, we also fabricated typical NP-DSSCs. These photoelectrodes were prepared using the established doctor-blade technique with commercially available TiO_2−NPs (Degussa P-25, average diameter ~25 nm).

The specific surface area and pore volume of TiO_2−NR and TiO_2−NP photoelectrodes were estimated by Brunauer−Emmett−Teller (BET) and Barrett−Joyner−Halenda (BJH) analysis using a nitrogen adsorption−desorption apparatus. The measured specific surface areas of TiO_2−NR photoelectrodes (123 $m^2\ g^{-1}$) were approximately two times greater than that observed for TiO_2−NP photoelectrodes (56.0 $m^2\ g^{-1}$). This indicates that TiO_2−NR photoelectrodes should provide larger sensitizer surface coverages than traditional TiO_2−NP photoelectrodes. To measure the surface coverage of sensitizers adsorbed to the surface of TiO_2, the surface-bound sensitizers were desorbed in 0.1 M NaOH (aq) to hydrolyze the carboxylate surface linkages.[13] The number of molecules was calculated from UV−vis absorption spectra of desorbed sensitizers using the extinction coefficient of the N719 sensitizer (ε = 3748 $cm^{-1}\ M^{-1}$ at 535 nm). It was determined that 8.59×10^{-8} mol of sensitizer molecules per mg of TiO_2 were attached to the surface of electrospun TiO_2−NRs compared to 3.44×10^{-8} mol mg^{-1} for TiO_2−NPs. The pore volumes for TiO_2−NRs and TiO_2−NPs were 1.28 and 0.61 $cm^3\ g^{-1}$, respectively. The higher pore volume observed for TiO_2−NRs is a result of the free volume that is created during the calcination step, in which a phase-segregated domain, PVAc, was removed from the TiO_2-gel/PVAc composite.

Figure 2a shows the incident photon to current efficiency (IPCE) results for NR-DSSCs and NP-DSSCs at the same photoelectrode thickness (12 μm). The quantum efficiency at 530 nm is larger by 12.5% for the NR-DSSCs. Due to their larger pore volume, the NR-based photoelectrodes contain approximately half the weight of TiO_2 at equal film thickness as compared to NP-based photoelectrodes. The NR-based photoelectrodes adsorb sensitizer molecules approximately 2.5 times more than the TiO_2−NP does. The sensitizer loadings at equal film thickness are similar for the two photoelectrode types.

Figure 2b shows the $J-V$ characteristics of the NR-DSSCs and NP-DSSCs. The NR-DSSCs showed a V_{oc}, J_{sc}, fill factor (FF), and power conversion efficiency (PCE) of 788 mV, 15.32 mA cm^{-2}, 74.5%, and 9.00%, respectively, at a photoelectrode thickness of ca. 12 μm; the NP-DSSCs gave 762 mV, 12.10 mA cm^{-2}, 67.0%, and 6.17% at the same thickness. The higher quantum efficiency and short circuit current density for the NR-DSSCs are tentatively attributed to a faster rate of electron transport through the single-crystalline TiO_2−NRs.

Generally, the photocurrent in DSSCs is determined by several factors such as the types of photoelectrode, sensitizer, and electrolyte that are utilized. The photoelectrode morphology can also influence photocurrent generation. One-dimensional TiO_2 nanostructures are believed to be a preferred morphology for DSSC photoelectrodes. The higher efficiency of photocurrent generation with 1D TiO_2 nanostructures has been explained by a reduction in grain boundaries,[14,15] higher dye loadings,[7,8] and slower recombination rates.[6] To understand the origin of higher short circuit current densities in our NR-DSSCs, the charge transport characteristics were investigated by intensity modulation photocurrent spectroscopy (IMPS) and intensity modulation photovoltage spectroscopy (IMVS). In both measurements, a delayed current or voltage response was recorded with respect

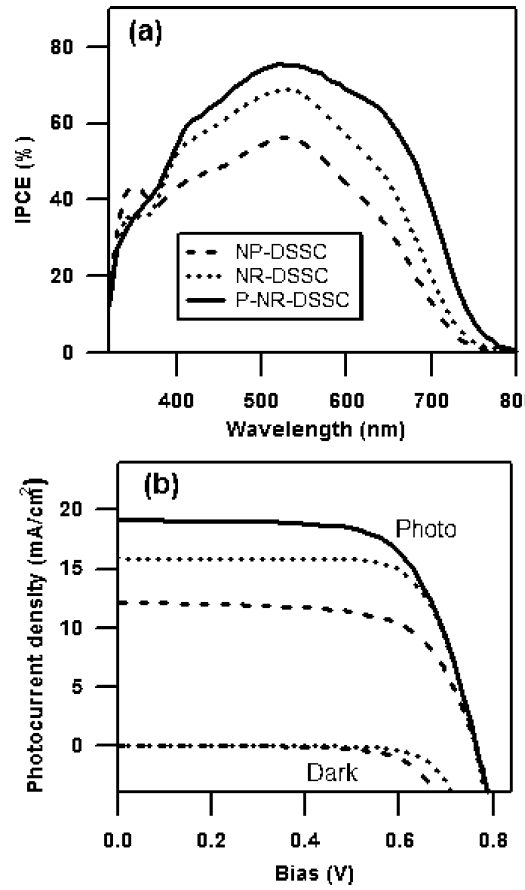

Figure 2. IPCE (a) and $J-V$ curves (b) of NP-DSSC, NR-DSSC, and P-NR-DSSC under simulated AM 1.5G light. The sample thickness is 12 μm.

to the frequency of incident light modulation in the range of 100−0.01 Hz. The time delay from IMPS measurements, τ_t, corresponds to the transport time of the injected electrons through the TiO_2 photoelectrode. The transport time can be estimated from the relation $\tau_t = \pi \cdot f_{D\min}/2$, where $f_{D\min}$ is the characteristic frequency at the minimum of the imaginary IMPS (Figure 3a). The electron diffusion coefficients, D_n, are determined from the equation $D_n = d^2/(2.35\tau_t)$[6,10] where d is the thickness of the photoelectrode. Figure 4a shows electron diffusion coefficients (D_n) of the DSSCs as a function of the incident photon flux (or light intensity absorbed by the sensitizers), I_o. It is noteworthy that the electron diffusion coefficients for NR-DSSCs were similar to that of NP-DSSCs even though the NR-based photoelectrodes contain approximately half the total TiO_2 weight at equal film thickness. This is an intriguing result when one considers the fact that the higher pore volume results in a more tortuous propagation of electrons, a higher number of electron trapping and detrapping events, and a longer overall electron transport time to the FTO current collector.[16−18] The similar electron diffusion coefficients for both types of DSSCs suggest that electron transport is faster in the single-crystalline NR-based DSSCs. Faster electron transport is presumably due to the presence of fewer grain boundaries and fewer interparticle junctions for the higher aspect ratio NRs.

The electron lifetimes within DSSCs are determined primarily by the recombination of electrons with iodine, electrolyte, and oxidized sensitizers. Using IMVS (Figure 3b), the recombination lifetime, τ_r, was determined using the relation $\tau_r = \pi \cdot f_{N\min}/2$, where $f_{N\min}$ is the characteristic frequency at the minimum of the IMVS imaginary component. Figure 4b shows that the

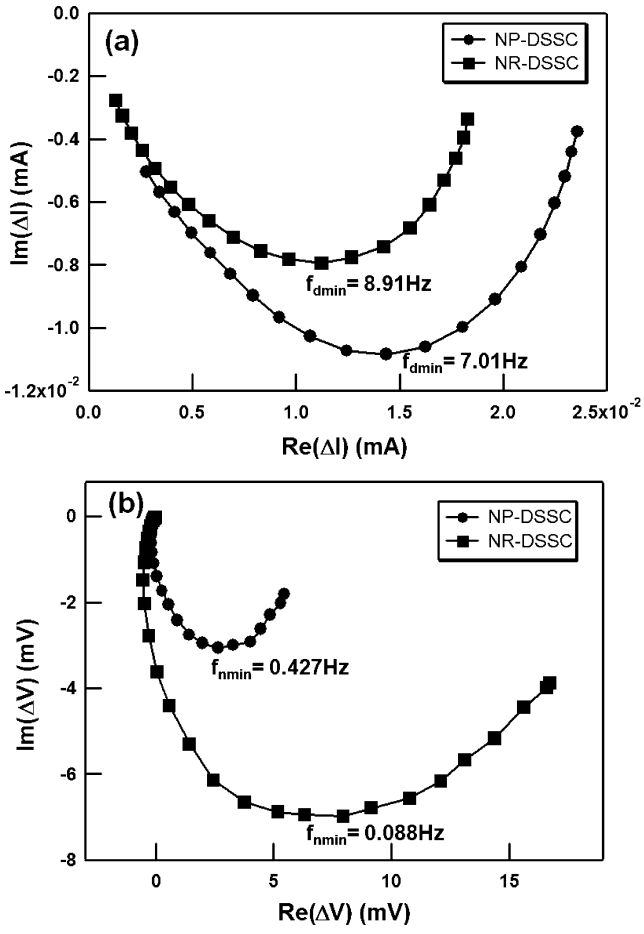

Figure 3. Typical IMPS (a) and IMVS (b) plots of NP-DSSC and NR-DSSC.

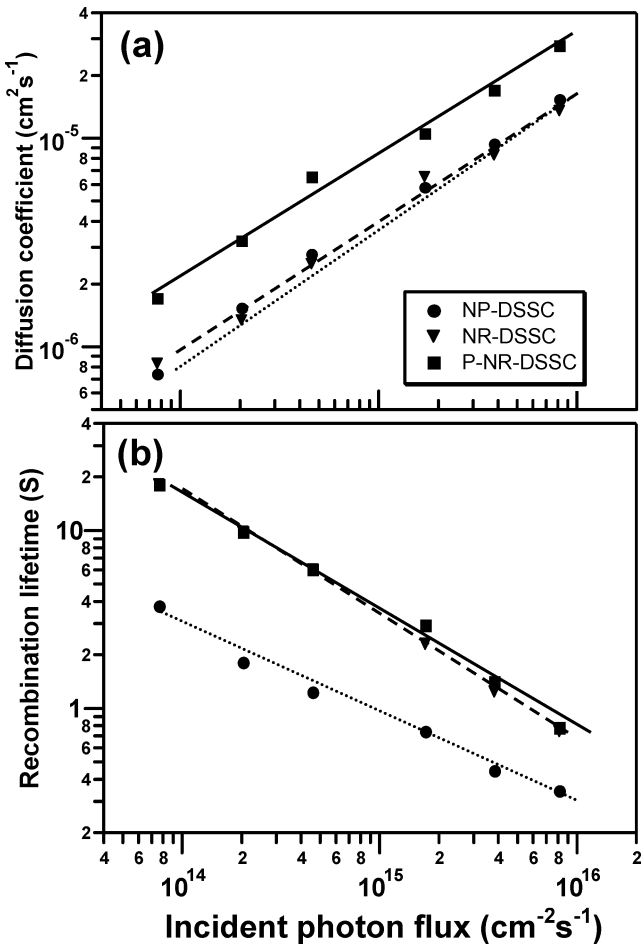

Figure 4. Electron diffusion coefficients (D_n) (a) and recombination lifetime (τ_r) (b) of NP-DSSC, NR-DSSC, and P-NR-DSSC as a function of the incident photon flux for 635 nm modulated (<1%) laser illumination.

recombination lifetime for NR-DSSCs is approximately eight times longer than that for NP-DSSCs. The relatively defect-free single-crystalline TiO_2−NRs have fewer grain boundaries which results in fewer electron trapping events at particle−particle interfaces.[5,8] Furthermore, the dark $J-V$ characteristics of NR-DSSCs showed a higher dark current onset (0.61 V) than that for NP-DSSC (0.51 V); this is consistent with fewer back reactions and slower recombination for NR-DSSCs.[4,6] The efficiency of charge collection is determined by the competition between recombination and transport of electrons within the photoanode. For most liquid electrolyte based DSSCs, charge transport is dominated by the diffusion of electrons in the absence of a significant electric field because of the photoelectrode dimensions and the high dielectric constant of the TiO_2 photoelectrode. The injected electrons within TiO_2 are screened by the high charge density of the electrolyte. The charge collection efficiency, η_{cc}, described by the relation[11] $\eta_{cc} = 1 - \tau_t/\tau_r$, was 21.5% greater for NR-DSSCs than that for NP-DSSCs at a light intensity (incident photon flux) of 8.1×10^{16} cm^{-2} s^{-1}. The relative competition between electron−hole recombination and electron diffusion is conveniently described by the electron diffusion length, L_n, and the relation $L_n = (D_n \cdot \tau_r)^{1/2}$.[19] The electron diffusion length is the average distance (normal to the plane of the film) an injected electron can travel through the photoelectrode prior to undergoing recombination.[20] If $L_n > d$ (where d is the TiO_2 photoelectrode thickness), only a small fraction of injected charge will be lost before it is collected; long diffusion lengths are therefore desirable. The average L_n values of NR- and NP-based photoelectrodes were estimated to be 11.4 and 6.1 μm, respectively. This suggests that electrons in TiO_2−NRs travel much further in comparison to those in TiO_2−NP.

From a morphological viewpoint, the 1D nanostructured TiO_2−NRs appear to allow for easier electron transport because they have fewer interparticle connections compared to TiO_2−NP systems. However, the significantly larger pore volume of our TiO_2−NR photoelectrodes resulted in an electron diffusion coefficient that was similar to what was observed for TiO_2−NP photoelectrodes. Since the diffusion coefficient is determined by the transport time along the thickness of the photoelectrode, the higher pore volume results in a longer average path length for electron percolation. Based on these results, one may expect that the electron diffusion can be enhanced by reducing the pore volume of TiO_2−NR photoelectrodes. To this end, the pores of TiO_2−NRs were partially filled by depositing TiO_2 in a post-treatment step.[21−25] The TiO_2−NRs were submerged in 0.05 M of $TiCl_4$ (aq) to grow TiO_2 onto the surface of the NRs. As the deposition proceeded, the pores of TiO_2−NR photoelectrodes were gradually filled. After 4 h of $TiCl_4$ treatment, the pore volume of TiO_2−NR photoelectrode was reduced to 0.83 cm^2 g^{-1}. The increase in the TiO_2 volume fraction concomitantly resulted in a ~10% enhancement in sensitizer adsorption.

The D_n of post-treated NR-DSSCs (P-NR-DSSC) was ca. 51% higher than that of untreated NR-DSSCs at a light intensity of 8.1×10^{16} cm^{-2} s^{-1}, in accordance with the observed increase (19%) in charge collection efficiency following the definition

TABLE 1: Characteristics of DSSCs Prepared from Various TiO_2 Photoelectrodes[a]

TiO_2	thickness (μm)	J_{sc} (mA cm^{-2})	V_{oc} (V)	FF (%)	η (%)
TiO_2−NP	12	12.10	0.762	67.0	6.17
TiO_2−NR	12	15.32	0.788	74.5	9.12
TiO_2−NR	14	16.52	0.772	74.6	9.50
P-TiO_2−NR	12	19.04	0.777	67.79	10.20
P-TiO_2−NR	14	21.07	0.770	68.4	11.09
P-TiO_2−NR (masked)	14	17.60	0.761	70.0	9.52

[a] All the measurements were collected without a mask except the noted sample.

mentioned above (Figure 4a). The TiO_2 post-treatment presumably enhances interparticle connectivity at NR grain boundaries and makes electron transport less obstructed by attenuating the scattering of free carriers. Electron transport enhancements in NR-DSSCs following $TiCl_4$ (aq) post-treatments have been reported previously and have been attributed to enhanced interparticle necking.[21−23] The recombination lifetime before and after the post-treatment remained the same. Improvements in the electron diffusion and sensitizer adsorption resulted in an increase in J_{sc} for P-NR-DSSC (19.27 mA cm^{-2}) compared to that for untreated NR-DSSC (15.32 mA cm^{-2}) at the same photoelectrode thickness (12 μm) (Figure 2b). As summarized in Table 1, the PCE of DSSCs using either NP, untreated NR, or $TiCl_4$-treated NR-based photoelectrodes at a constant thickness of ca. 12 μm were 6.17%, 9.12%, and 10.20%, respectively. The IPCEs for P-NR-DSSCs were approximately 8.3% higher than that for untreated NR-DSSCs in the 350−800 nm wavelength range (Figure 2a). In the long wavelength region (650−750 nm), the gain in IPCE for P-NR-DSSCs increased up to 14% due to light scattering effects. These results are consistent with a larger amount of adsorbed sensitizers and a higher electron diffusion coefficient.

Finally, we investigated the effect of film thickness on the PCEs of NR-DSSCs. The PCEs of DSSCs increase linearly until the photoelectrode thickness reaches 14 μm, in accordance with IMPS results. The optimized PCEs of DSSCs at a film thickness of 14 μm were 9.50% for untreated NR-DSSCs (V_{oc} = 772 mV, J_{sc} = 16.52 mA cm^{-2}, FF = 74.6%) and 11.09% for P-NR-DSSCs (V_{oc} = 770 mV, J_{sc} = 21.07 mA cm^{-2}, FF = 68.4%). We also measured the $J-V$ characteristics and IPCE using the shading mask method[26] that has been used to limit photocurrent overestimation arising from light-guiding effects that occur as light passes through the conductive glass electrode. Under these conditions, the following results were obtained for P-NR-DSSCs with a film thickness of 14 μm: V_{oc} = 761 mV, J_{sc} = 17.6 mA cm^{-2}, fill factor = 70.0%, and an overall efficiency of 9.52%.

Conclusions

In summary, highly efficient DSSCs were fabricated using TiO_2−NR-based photoelectrodes prepared by a combination of sol−gel chemistry and electrospinning. Their charge transport properties were investigated and compared with those of typical NP-based TiO_2 photoelectrodes. The electrospun TiO_2−NR-based photoelectrodes had twice the pore volume of TiO_2−NP (P25)-based photoelectrodes and gave ∼2.5 times higher sensitizer surface coverages at the same weight of TiO_2. They exhibited higher energy conversion efficiencies than NP-DSSCs because the two systems have similar electron diffusion coefficients and electron−hole recombination is more than eight times slower in NR-DSSCs. The electron transport behavior of NR-DSSCs was further improved by $TiCl_4$ post-treatment. The post-treatment reduces the pore volume of NR-based photoelectrodes while improving inter-rod connectivity and enhancing electron diffusion. The electron diffusion coefficient of P-NR-DSSCs was ∼51% higher than that of untreated NR-DSSCs, leading to a charge collection efficiency that was 19% higher at a photon flux of 8.1 × 10^{16} cm^{-2} s^{-1}. Finally, the efficiency of nanorod-based DSSCs was optimized at a photoelectrode thickness of 14 μm to achieve 9.52% under masked illumination of simulated solar light, AM 1.5 global (V_{oc} = 761 mV, J_{sc} = 17.6 mA cm^{-2}, fill factor = 70.0%).

Acknowledgment. This work was supported by KIST Institutional Program (Grant No. 2E20980). The authors thank Dr. N.-G. Park for the IPCE measurements and helpful discussions.

References and Notes

(1) O'Regan, B.; Grätzel, M. *Nature* **1991**, *353*, 737–740.
(2) Bisquert, J.; Cahen, D.; Hodes, G.; Rühle, S.; Zahan, A. *J. Phys. Chem. B* **2004**, *108*, 8106–8118.
(3) Gregg, B. A.; François, F.; Ferrere, S.; Fields, C. L. *J. Phys. Chem. B* **2001**, *105*, 1422–1429.
(4) Kopidakis, N.; Benkstein, K. D.; van de Lagemaat, J.; Frank, A. J. *J. Phys. Chem. B* **2003**, *107*, 11307–11315.
(5) Jiu, J.; Isoda, S.; Wang, F.; Adachi, M. *J. Phys. Chem. B* **2006**, *110*, 2087–2092.
(6) Zhu, K.; Neale, N. R.; Miedaner, A.; Frank, A. J. *Nano Lett.* **2007**, *7*, 69–74.
(7) Adachi, M.; Murata, Y.; Liu, J.; Sakamoto, M.; Wang, F. *J. Am. Chem. Soc.* **2004**, *126*, 14943–14949.
(8) Kang, S. H.; Choi, S.-H.; Kang, M.-S.; Kim, J.-Y.; Hyeon, T.; Sung, Y.-E. *Adv. Mater.* **2008**, *20*, 54–58.
(9) Song, M. Y.; Ahn, Y. R.; Jo, S. M.; Kim, D. Y. *Appl. Phys. Lett.* **2005**, *87*, 113113.
(10) van de Lagemaat, J.; Frank, A. J. *J. Phys. Chem. B* **2001**, *105*, 11194–11205.
(11) Schlichthörl, G.; Park, N.-G.; Frank, A. J. *J. Phys. Chem. B* **1999**, *103*, 782–791.
(12) Song, M. Y.; Kim, D. K.; Ihn, K. J.; Jo, S. M.; Kim, D. Y. *Nanotechnology* **2004**, *15*, 1861–1865.
(13) Nazeeruddin, M. K.; Kay, A.; Rodicio, I.; Humphry-Baker, R.; Müller, E.; Liska, P.; Vlachopoulos, N.; Grätzel, M. *J. Am. Chem. Soc.* **1993**, *115*, 6382–6390.
(14) Fujihara, K.; Kumar, A.; Jose, R.; Ramakrishna, S.; Uchida, S. *Nanotechnology* **2007**, *18*, 365709.
(15) Baxter, J. B.; Aydil, E. S. *Sol. Energy Mater. Sol. Cells* **2006**, *90*, 607–622.
(16) Liang, L.; Dai, S.; Hu, L.; Kong, F.; Xu, W.; Wang, K. *J. Phys. Chem. B* **2006**, *110*, 12404–12409.
(17) Benkstein, K. D.; Kopidakis, N.; van de Lagemaat, J.; Frank, A. J. *J. Phys. Chem. B* **2003**, *107*, 7759–7767.
(18) Cass, M. J.; Walker, A. B.; Martinez, D.; Peter, L. M. *J. Phys. Chem. B* **2005**, *109*, 5100–5107.
(19) Bandić, Z. Z.; Bridger, P. M.; Piquette, E. C.; McGill, T. C. *Appl. Phys. Lett.* **1998**, *73*, 3276.
(20) Barnes, P. R. F.; Anderson, A. Y.; Koops, S. E.; Durrant, J. R.; O'Regan, B. C. *J. Phys. Chem. C* **2009**, *113*, 1126–1136.
(21) Barbé, C. J.; Arendse, F.; Comte, P.; Jirousek, M.; Lenzmann, F.; Shklover, V.; Grätzel, M. *J. Am. Ceram. Soc.* **1997**, *80*, 3157–3171.
(22) Park, N.-G.; Schlichthorl, G.; Van de Lagemaat, J.; Cheong, H. M.; Mascarenhas, A.; Frank, A. J. *J. Phys. Chem. B* **1999**, *103*, 3308–3314.
(23) Mor, G. K.; Shankar, K.; Paulose, M.; Varghese, O. K.; Grimes, C. A. *Nano Lett.* **2006**, *6*, 215–218.
(24) Zhang, D.; Ito, S.; Wada, Y.; Kitamura, T.; Yanagida, S. *Chem. Lett.* **2001**, *30*, 1042–1043.
(25) Kambe, S.; Nakade, S.; Wada, Y.; Kitamura, T.; Yanagida, S. *J. Mater. Chem.* **2002**, *12*, 723–728.
(26) Ito, S.; Nazeeruddin, M. K.; Liska, P.; Comte, P.; Charvet, R.; Péchy, P.; Jirousek, M.; Kay, A.; Zakeeruddin, S. M.; Grätzel, M. *Prog. Photovolt: Res. Appl.* **2006**, *14*, 589–601.

JP907855X